Böhnke, H., Roettger, K., Ingle, R., Marroux, H., Bohnsack, M., Schwalb, N., Orr-Ewing, A., & Temps, F. (2019). Electronic Relaxation Dynamics of UV-Photoexcited 2-Aminopurine–Thymine Base Pairs in Watson-Crick and Hoogsteen Conformations. *Journal of Physical Chemistry B*, *123*(13), 2904-2914. https://doi.org/10.1021/acs.jpcb.9b02361

Electronic Relaxation Dynamics of UV-Photoexcited 2-Aminopurine–Thymine Base Pairs in Watson–Crick and Hoogsteen Conformations

Hendrik Böhnke,[a] Katharina Röttger,[1ab] Rebecca A. Ingle,[2b] Hugo J. B. Marroux,[3b]

Mats Bohnsack,[a] Nina K. Schwalb,[4a] Andrew J. Orr-Ewing[b] and Friedrich Temps*[a]*

[a] Institute of Physical Chemistry, Christian-Albrechts-University Kiel, Olshausenstr. 40, 24098 Kiel, Germany

[b] School of Chemistry, University of Bristol, Cantock's Close, Bristol BS8 1TS, UK

[1] Current address: Centre for Process Innovation, Wilton Centre, Wilton, Redcar TS10 4RF, UK

[2] Current address: École Polytechnique Fédérale de Lausanne, Laboratoire de Spectroscopie Ultrarapide (LSU) and Lausanne Centre for Ultrafast Science (LACUS), ISIC, FSB, 1015 Lausanne, Switzerland

[3] Current address: Chemical Sciences Department, Lawrence Berkeley National Laboratory, 1 Cyclotron Road, Berkeley, CA 94720, USA

[4] Current address: Bayer AG, Consumer Health Division, 51368 Leverkusen, Germany

ABSTRACT

The fluorescent analogue 2-aminopurine (2AP) of the canonical nucleobase adenine (6-aminopurine) base-pairs with thymine (T) without disrupting the helical structure of the DNA. It therefore finds frequent use in molecular biology for probing DNA and RNA structure and conformational dynamics. However, detailed understanding of the processes responsible for fluorescence quenching remains largely elusive on a fundamental level. While attempts have been made to ascribe decreased excited-state lifetimes to intra-strand charge transfer and stacking interactions, possible influences from dynamic inter-strand H-bonding have been widely ignored. Here, we investigate the electronic relaxation of UV-excited 2AP·T in Watson–Crick (WC) and Hoogsteen (HS) conformations. While the WC conformation features slowed-down, monomer-like electronic relaxation in $\tau \sim 1.6$ ns towards ground-state recovery and triplet formation, the dynamics associated with 2AP·T in the HS motif exhibit faster deactivation in $\tau \sim 70$ ps. As recent research has revealed abundant transient inter-strand H-bonding in the Hoogsteen motif for duplex DNA, the established model for dynamic fluorescence quenching may need to be revised in the light of our results. The underlying supramolecular photophysical mechanisms are discussed in terms of a proposed excited-state double proton transfer as an efficient deactivation channel for recovery of the HS species in the electronic ground state.

INTRODUCTION

2-Aminopurine (2AP) is a fluorescent analogue of the canonical nucleobase adenine that base-pairs with thymine (T) with little perturbation of the helical structure when incorporated into DNA.[1-7] Since its fluorescence lifetime is highly sensitive to the molecular microenvironment,[8-15] it is widely used in DNA and RNA studies as a weakly perturbing probe for monitoring solvation[9] and conformational dynamics,[12,13,16,17] base stacking/unstacking interactions,[11,12,18-20] nucleotide binding and exchange,[21] and charge transfer processes.[22-24] Photoexcitation at $\lambda = 310$ nm selectively addresses the 2AP chromophore owing to the red-shift of its first $^1\pi\pi^*$ electronic absorption band in the ultraviolet (UV) compared to the spectra of the canonical nucleobases. However, understanding the complex electronic relaxation mechanisms in photoexcited oligonucleotides continues to present challenges due to competing intra-strand deactivation dynamics induced via charge-transfer and stacking interactions, including exciton and excimer formation, and inter-strand de-excitation via H-bonded base pairs.[25-30] Moreover, as recently discovered, duplex DNA also contains transient Hoogsteen base pairs as additional structural motifs to enhance functional versatility beyond the Watson-Crick limitations,[31,32] further complicating the dynamics of photoexcited DNA, especially when containing 2AP.

Here, we report on the electronic deactivation pathways in purely H-bonded 2AP·T base pairs in Watson–Crick (WC) and Hoogsteen (HS) conformations after selective UV photoexcitation of the 2AP chromophore. Our investigations used femtosecond transient vibrational absorption spectroscopy (TVAS), a method sensitive not only to molecular structure but also to the characters of the excited electronic states. To assure sufficient concentrations of 2AP·T, we studied the tert-butyldimethylsilyl (TBDMS) protected nucleoside of 2AP and the respective protected 2'-deoxy-

nucleoside of T in chloroform ($CHCl_3$) solution. For simplicity, the free 2AP riboside, the free T 2'-deoxyriboside and their H-bonded pairs are henceforth referred to as 2AP, T, T·T and 2AP·T.

METHODS

Time-resolved spectroscopy

Time-resolved measurements upon UV excitation were performed using 25 mM equimolar sample concentrations of 2AP and T at an optical pathlength of 100 μm. $CHCl_3$ was chosen as solvent as it features a dielectric environment similar to that in the DNA double helix[33] and ensures a high optical transmission in the mid-infrared (mIR) spectrum. To enable sufficient solubility of 2AP and T in such an apolar solvent, the riboside OH groups of the nucleoside and 2'-deoxy-nucleoside, respectively, were protected by bulky, apolar *tert*-butyldimethylsilyl (TBDMS) groups. Association constants for hetero-dimer formation ($K_{2AP\cdot T}$) and homo-dimer formation ($K_{T\cdot T}$) were determined by concentration-dependent static ground-state vibrational spectroscopy (cf. Fig. 1) using a Bruker IFS 66v Fourier-transform infrared (FTIR) spectrometer.

Time-resolved transient vibrational absorption measurements of UV-photoexcited molecules were performed at the University of Bristol.[34] Excitation pulses at $\lambda_{pump} = 310$ nm with duration of ~ 100 fs (full width at half maximum) were generated by a Coherent OPerA Solo optical parametric amplifier (OPA) pumped by 2.45 mJ per pulse from a Coherent Legend Elite HE+ regenerative amplifier running at 1 kHz and 800 nm with 40 fs duration. The pump pulses were attenuated to 100 nJ per pulse (2AP) and 200 nJ per pulse (2AP + T) by a combination of a λ/2 waveplate and a wire-grid polarizer and set to the magic angle condition (54.7°) with respect to the probe pulses. The doubled excitation energy for the measurements of the 2AP + T mixture

relative to the measurements of the free monomer accounts for the lower effective excited-state concentration of free 2AP in the mixture (~50 %). Thus, no further weighting was necessary in the subtraction of the TVA spectra of 2AP from the spectra of the 2AP + T mixture (see later). Broadband mIR probe pulses were supplied by difference frequency generation of the signal and idler from a second OPA, giving tunable pulses with ~ 300 cm^{-1} bandwidth in the 1250–4000 cm^{-1} range. After passing through the sample, the mIR probe pulses were spectrally dispersed in a grating spectrograph (HORIBA Scientific, iHR320) and detected on a 128 pixel, liquid N_2-cooled mercury cadmium telluride array (Infrared Associates). For transient measurements, the UV pump pulses were delayed using an aluminium retro-reflector mounted on a motorized delay stage and modulated at 0.5 kHz with an optical chopper wheel for pump-on/pump-off pairs of spectra.

The supplementary time-resolved fluorescence measurements to determine the excited-state lifetimes of 2AP·T in $CHCl_3$ were performed using the up-conversion setup in Kiel.[35]

Computational methods

Quantum chemical calculations were carried out to derive the energetic order of the excited electronic states above the FC geometry of the GS and to assign the characteristic vibrational marker bands observed in the FTIR and time-resolved TVA spectra. To save computer time, the protected riboside residue was substituted by a methyl group in all calculations. Relaxed GS structures and vibrational frequencies were determined by DFT calculations with the M062X functional[36] in combination with the 6-311+G** basis set[37-40] using the Gaussian09 suite of programs[41] for free 2AP, free T, T·T homo-dimers and 2AP·T hetero-dimers. The calculated wavenumbers were scaled[42,43] to obtain best agreement with the experimental data using factors of 0.955 and 0.94 below and above 2000 cm^{-1}, respectively, as done before for the 2AP monomer.

The relative energies of the different species were obtained by DFT calculations at the B2PLYP-D3(BJ)[44]/def2-QZVP[45] level of theory employing the Turbomole 7.0 program.[46] The B2PLYP-D3(BJ) double hybrid method was chosen because it has recently been shown in a series of benchmark calculations[44,47,48] to provide more accurate results than the common B3LYP functional.

Complementary calculations were run using second-order Møller–Plesset perturbation theory (MP2) under the resolution of the identity (RI) approximation[49-52] with the def2-TZVPPD basis set[53-55] to obtain starting points for the excited states. Vertical excitation energies (VEEs) were then computed using the second-order approximation coupled-cluster (CC2) method in Turbomole 7.0 in the form of the RI-CC2[56-61] variant with the def2-TZVPPD basis set. Excited-state properties such as equilibrium structures and associated vibrational mode frequencies for the $^1\pi\pi^*$ and $^3\pi\pi^*$ state minima were computed for free 2AP.[62] The obtained vibrational wavenumbers in the excited states were scaled with factors of 0.99 and 0.94 below and above 2000 cm^{-1}, respectively,[63] to obtain best agreement between the calculated and measured transient vibrational spectra. To mimic the vibrational spectra in the region of ring vibrations in the electronically excited states of 2AP·T, the calculated spectra for free 2AP were scaled to match the observed transient features with a factor of 0.975. Geometry relaxations and VEEs at frozen N-H distances in the 2AP·T dimers in the WC and HS conformations were carried out under the resolution of the identity approximation at the MP2 (GS) and ADC(2)[64] ($^1\pi\pi^*$) levels of theory employing the def2-SVP basis set.[53]

RESULTS

Association equilibria between 2AP, T, T·T and 2AP·T

H-bonded 2AP·T co-exists in concentration-dependent equilibria with free 2AP, free T and T·T dimers in $CHCl_3$ solution. As illustrated in Fig. 1, characteristic vibrational marker bands of 2AP, T, T·T and 2AP·T were identified in measured Fourier-transform infrared (FTIR) spectra and assigned aided by quantum chemical calculations. Investigation of the spectral region from 3600 – 3150 cm^{-1} in Fig. 1 reveals vibrational bands at 3532 (3544) cm^{-1} and 3424 (3423) cm^{-1} associated with the antisymmetric and symmetric NH_2 stretching modes of 2AP (calculated values in parentheses) both in the spectra of 2AP and the 2AP+T mixture. Also, the 2AP+T mixture shows vibrational modes of T at 3398 (3397) cm^{-1} and 3201 (3181) cm^{-1} associated with the NH stretching mode of free T and homo-dimeric T·T, respectively. By following these vibrational marker bands in concentration-dependent studies, we determined the specific association constants $K_{T\cdot T} = 2.1 \pm 0.7\ M^{-1}$ for the equilibrium between T and T·T,[65] and $K_{2AP\cdot T} = 60 \pm 17\ M^{-1}$ for the equilibrium between 2AP, T and 2AP·T. No evidence was found for significant self-association of 2AP in the investigated concentration range. Also, justified by the choice of $CHCl_3$ as solvent, no indications of stacked chromophores were obtained in the FTIR and UV/vis spectra (Figs. 1 and 3). With these premises, taking the association constants $K_{T\cdot T}$ and $K_{2AP\cdot T}$, the percentage amount of H-bonded 2AP·T in a mixture of 2AP and T can readily be calculated. In a mixture of 2AP + T at initial concentrations of $c_0(2AP) = c_0(T) = 25$ mM as used in all time-resolved dynamics measurements in this work, the molar fractions of the constituents are calculated as $x_{2AP\cdot T} = 0.29$, $x_{2AP} = 0.36$, $x_T = 0.34$, and $x_{T\cdot T} = 0.01$. Thus, we calculate the free bases 2AP and T, and hetero-dimeric 2AP·T to be the dominating species in our sample solutions, while homo-dimeric T·T

contributes only insignificantly to the FTIR spectra owing to the low association constant for self-association of T.

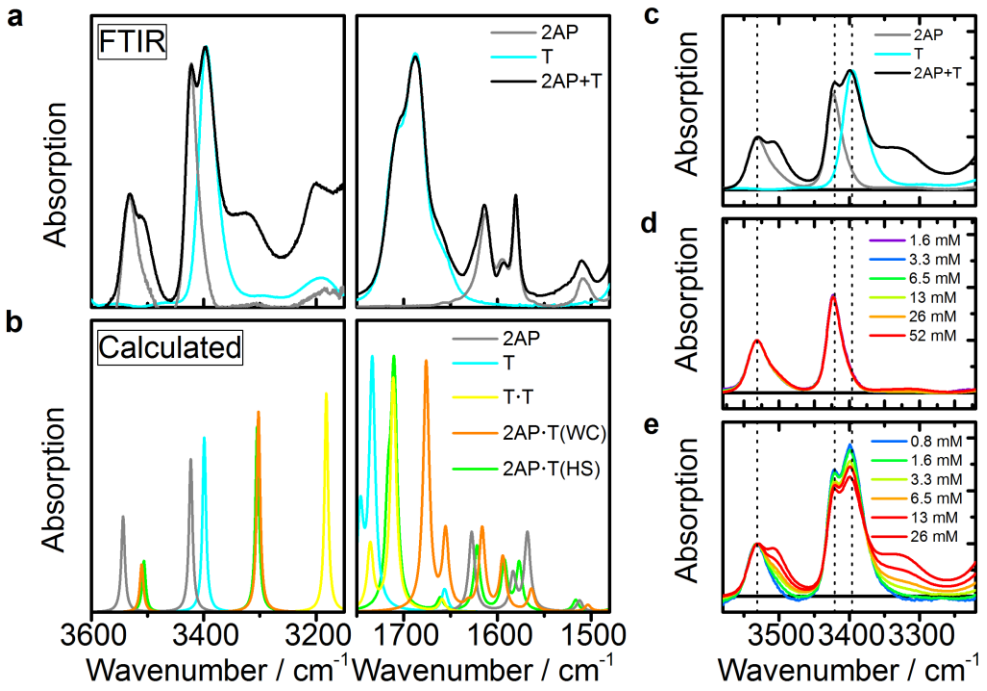

Figure 1. FTIR spectra of 2AP, T and the 2AP+T mixture, computed vibrational modes and association constants. (a) FTIR spectra of 2AP (grey), T (cyan) and a mixture of 2AP and T (2AP + T, black) in $CHCl_3$ solution. (b) Calculated (M062X/6-311+G**) vibrational spectra of 2AP (grey), T (cyan), homo-dimeric T·T (yellow) and hetero-dimeric 2AP·T in the Watson–Crick (WC, orange) and in the Hoogsteen (HS, green) conformation. For clarity, only the most stable T·T dimer (-55.4 kJ/mol) is shown and the spectra for rWC and rHS are omitted. (c) FTIR spectra of free 2AP, free T and the 2AP + T mixture to highlight the characteristic 2AP·T dimer marker bands in the NH_2 stretching region. (d) Normalized FTIR spectra of free 2AP at different concentrations to exclude self-association. (e) FTIR spectra of equimolar mixtures of 2AP and T at different concentrations to obtain the association constant of H-bonded 2AP·T dimers.

In order to gain further insight into the structural diversity of the subset of hetero-dimeric 2AP·T, we employed quantum chemical calculations at the B2PLYP-D3(BJ)/def2-QZVP level of theory (corresponding to 0 K dissociation energies without zero-point energy or solvent correction). As depicted in Fig. 2, our calculations revealed very similar binding energies for the 2AP·T dimer in the Watson–Crick (WC), reverse-Watson–Crick (rWC), Hoogsteen (HS) and reverse-Hoogsteen (rHS) conformations, thus hinting at a rather diverse distribution of H-bonded 2AP·T dimers in WC and HS conformations. As has been shown elsewhere,[66] the Wobble conformation of 2AP·T is energetically less favoured and therefore neglected here. Note that rather crude gas-phase computations neglecting solvent effects, zero-point energies and steric effects of the TBDMS residue can provide only limited information on the actual distribution of H-bonded species. However, the characterization of exact thermodynamic distributions within the 2AP+T mixture is beyond the scope of this work. Still, justified by the emergence of distinct time constants for electronic deactivation in our time-resolved measurements below, our calculations tentatively hint at a rather heterogeneous distribution of WC and HS conformations at room temperature in $CHCl_3$ solution. Because they were indistinguishable in our experiments due to their structural similarities, the WC and rWC conformations on the one hand and the HS and rHS conformations on the other will be referred to simply as WC and HS conformations, respectively.

Fortunately, the rather complex distribution of free 2AP, free T and dimeric 2AP·T species gets significantly reduced for time-resolved experiments by selective photoexcitation of the 2AP chromophore both in free 2AP and within the 2AP·T framework. As can be seen from the UV absorption spectra of 2AP, T and the 2AP + T mixture in Fig. 3a, only the 2AP chromophore is excited at $\lambda_{pump} = 310$ nm. Accordingly, calculated vertical excitation energies revealed no significant red-shift of the optically bright electronic transitions of the T moiety upon H-bonding

with 2AP (cf. Fig. 3b and Supplementary Table S1). As elaborated above, the 2AP+T mixture consists of 2AP (36 %), T (34 %), T·T (1 %) and 2AP·T (29 %) in the electronic ground state. Assuming unchanged electronic transitions of 2AP upon H-bonding with T, this would translate to ~ 55 % photoexcited 2AP and ~ 45 % photoexcited 2AP·T. However, the first excited $^1\pi\pi^*$ state of the 2AP moiety within the 2AP·T framework is computed to exhibit a red-shift for both WC and HS conformations at comparable oscillator strengths (cf. Table S1). Thus, excitation at 310 nm leads to ~ 50 % photoexcited free 2AP and ~ 50 % photoexcited base-paired 2AP·T (WC and HS). Hence, contributions by free T and dimeric T·T[65] to the dynamics signals in the time-resolved measurements are safely negligible.

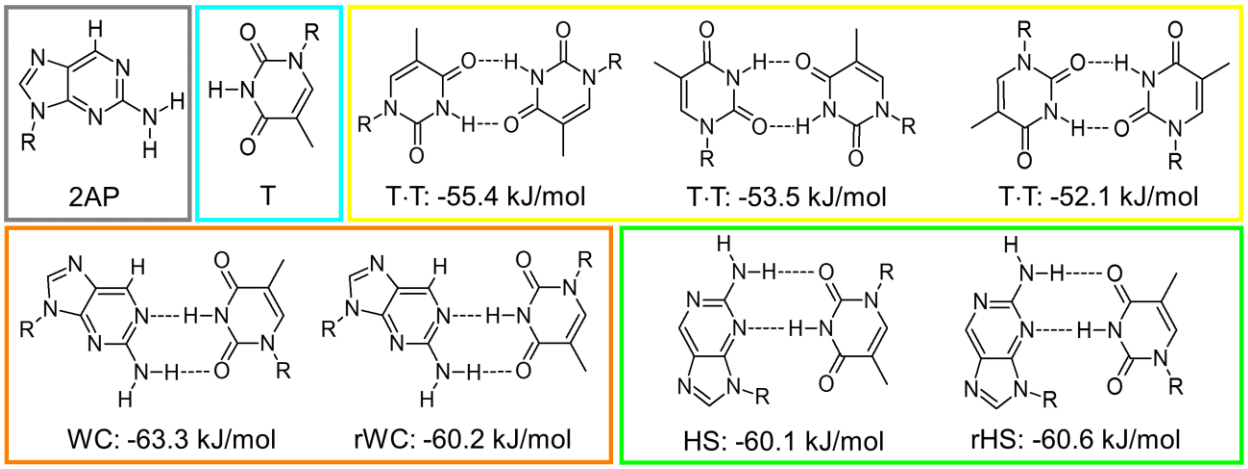

Figure 2. Molecular species present in the 2AP + T mixture. Monomeric, homo-dimeric and hetero-dimeric molecular species in the mixture of 2AP and T in $CHCl_3$ solution with calculated (0 K, isolated dimer) binding energies at the B2PLYP-D3(BJ)/def2-QZVP level of theory for the minimum energy structures obtained at the M062X/6-311+G** level of theory. The riboside residue (-R) was substituted by a methyl group in all calculations.

Time-resolved measurements

As a first test for dimer-specific electronic relaxation pathways in H-bonded 2AP·T, Fig. 3 shows time-resolved experimental fluorescence decay curves after 310 nm photoexcitation of solutions of free 2AP (Fig. 3c) and 2AP + T (Fig. 3d). For free 2AP, the measurement reveals minor initial Franck-Condon (FC) and solvational relaxation dynamics on a timescale of

$$\tau_{solv} = 3.0 \pm 1.0 \text{ ps}$$

followed by depopulation of the prepared optically bright $^1\pi\pi^*$ state with a time constant of

$$\tau_{2AP} = 740 \pm 15 \text{ ps.}$$

Since the 2AP + T solution consists of effectively ~ 50 % photo-excited free 2AP, the time-resolved fluorescence data consequentially exhibit a sizable signature of τ_{2AP} as well. However, the observed temporal evolution of the fluorescence clearly features two additional time constants,

$$\tau_{1,2AP\cdot T} = 44 \pm 10 \text{ ps}$$

and

$$\tau_{2,2AP\cdot T} = 1.9\ ^{+6}_{-1.9} \text{ ns,}$$

in addition to the contribution by free 2AP. Thus, despite the moderate (~ 50 %) excited-state fraction of dimeric 2AP·T species in the 2AP + T mixture, the observed temporal fluorescence profiles clearly reveal new dynamics that can arise only from H-bonded 2AP·T in either the WC or HS conformations or both.

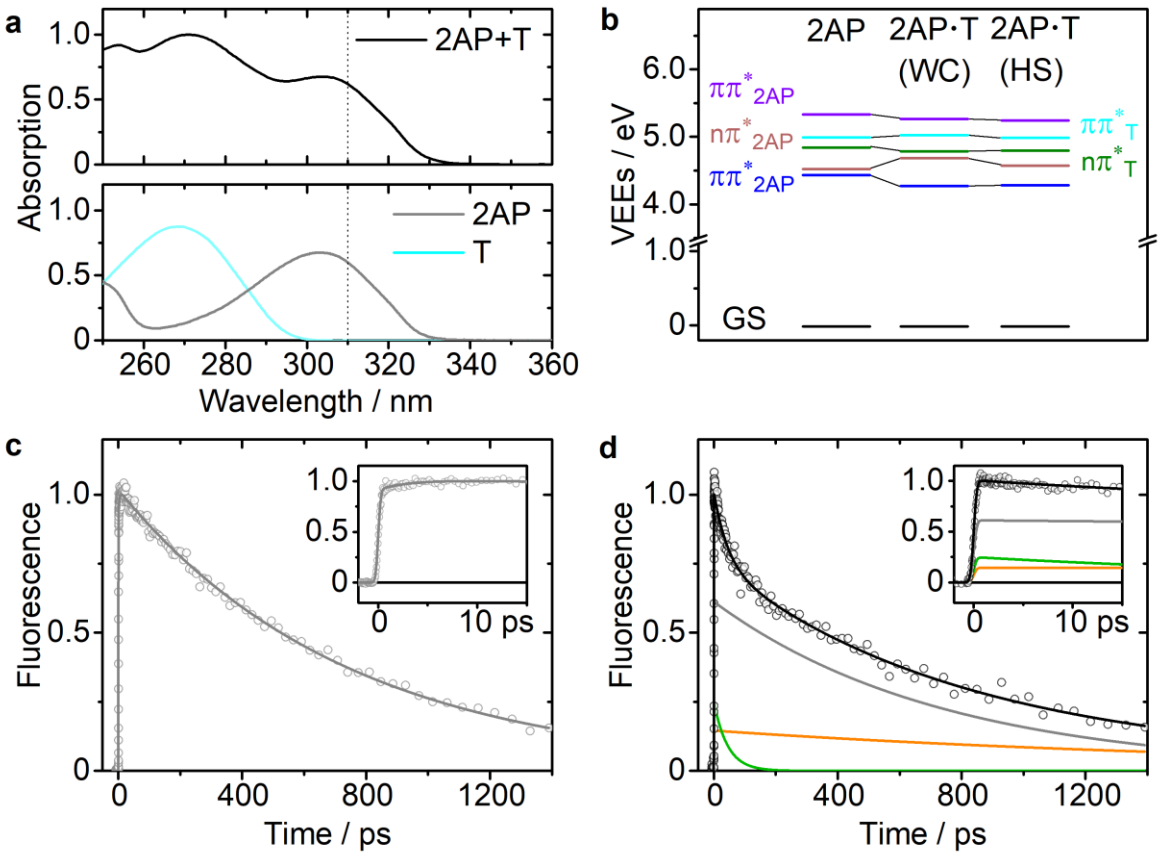

Figure 3. Electronic absorptions and time-resolved fluorescence of 2AP, T and 2AP·T. (a) UV absorption spectra of 2AP (grey), T (cyan) and a mixture of 2AP and T (2AP + T, black) in $CHCl_3$ solution. (b) Calculated vertical excitation energies (VEEs) at the RI-CC2/def2-TZVPPD level of theory for free 2AP and H-bonded Watson–Crick (WC) and Hoogsteen (HS) 2AP·T dimers, respectively, at the RI-MP2/def2-TZVPPD optimized ground-state structures. (c) Transient fluorescence–time profile of free 2AP measured at λ_{FL} = 410 nm after photoexcitation at λ_{pump} = 310 nm. Open circles are data points, the solid line is the least-squares best fit curve with τ = 740 ps. (d) Transient fluorescence–time profile of the 2AP+T mixture measured at λ_{FL} = 410 nm after excitation at λ_{pump} = 310 nm. The solid black line is the least-squares best fit curve with components of $\tau_{1,2AP\cdot T}$ = 44 ps (green), τ_{2AP} = 740 ps (grey) and $\tau_{2,2AP\cdot T}$ = 1.9 ns (orange).

As neither transient fluorescence nor transient electronic absorption spectroscopy provide sufficient chemical structure specificity, we use transient vibrational absorption spectroscopy (TVAS) in combination with quantum chemical vibrational mode calculations as methods of choice for identifying the 2AP·T species and electronic states involved in the dynamics. The results are displayed in Figs. 4 and 5.

We first isolate the features related to the free chromophore in the 2AP + T mixture after UV excitation. Towards these ends, we turn to our recent work on the electronic deactivation of 2AP in $CHCl_3$[62] and a preceding study by Reichardt et al.[67] In short, the relaxation pathways of free 2AP were identified from the temporal evolutions of a number of characteristic vibrational marker bands in the electronic ground and excited states. The spectral region of the NH_2 stretching vibrations proved to be especially valuable (cf. Fig. 4a). At early times after excitation, the TVA spectra feature two negative bands at 3532 and 3424 cm^{-1} associated with the bleached antisymmetric (as) and symmetric (s) NH_2 stretching modes in the electronic ground state (GS; see Fig. 5). Positive transients showing up at 3479 and 3356 cm^{-1} are indicative for the NH_2(as) and NH_2(s) stretching modes in the photoexcited $^1\pi\pi^*$ state. Concurrent with the $^1\pi\pi^*$ state depopulation and GS recovery, a transfer to the $^3\pi\pi^*$ state is witnessed by the rise of transient vibrational bands at 3500 and 3395 cm^{-1} at later times. Summarizing the conclusions for free 2AP, depopulation of the photoexcited $^1\pi\pi^*$ state is initiated by a fast population transfer to the lower-lying, short-lived, $^1n\pi^*$ state, for which an upper limit for its lifetime of $\tau \leq 100$ ps was estimated. From there, the excited molecules evolve partly to recover the GS (58 % in $CHCl_3$) and partly via intersystem crossing (ISC) to the $^3\pi\pi^*$ state (42 %). The rate-limiting step in the mechanism that gives rise to the observed 740 ps time constant τ_{2AP} is the $^1\pi\pi^*/^1n\pi^*$ internal conversion.[62]

TVA data were analyzed by fitting the experimental marker bands in different electronic states to a sum of Gaussian functions in a global fashion. Showcasing data analysis of TVA spectra for free 2AP in the spectral region of NH_2 stretching vibrations in Fig. 4a, a sum of six Gaussians – indicated by coloured arrows – was used to model the experimentally observed features. In the region from 3600 – 3200 cm^{-1}, the transient spectra are described by two negative, yet recovering Gaussians at 3532 (3544) cm^{-1} and 3424 (3423) cm^{-1} associated with initial ground-state bleaching and subsequent incomplete recovery (calculated values in parentheses). Additionally, the transient TVA spectra were described by a pair of Gaussians at 3479 (3493) cm^{-1} and 3356 (3342) cm^{-1} corresponding to the initially excited $^1\pi\pi^*$ state. Finally, the transient spectra were modelled by an additional pair of Gaussians at 3500 (3530) cm^{-1} and 3395 (3382) cm^{-1} to account for the rise of transient features towards late delay-times associated with $^3\pi\pi^*$ formation. In order to gain insight into the temporal evolution of the fitted transient marker bands, the associated Gaussian amplitudes at various delay times can be plotted as individual time profiles. Aided by quantum chemical calculations, however, Gaussian amplitudes of related vibrational marker bands have been coupled by a time-independent factor throughout description of the temporal evolution of the TVA spectra. Thus, the overall spectral shape of distinct spectroscopic species is described by subsets of coupled Gaussian functions. As a result, data analysis shifts from temporal description of individual bands towards the time-resolved description of the dynamics of underlying electronic states, effectively reducing the number of time-profiles and stabilizing the fitting procedure significantly in the process. Hence, Fig. 4a features three effective time profiles (ground-state recovery (grey), $^1\pi\pi^*$ decay (blue) and $^3\pi\pi^*$ formation (red)) for the description of the spectral region from 3600 – 3200 cm^{-1}. Further, the spectral region from 1650 – 1475 cm^{-1} has been modelled accordingly. In a final step, accounting for all time profiles in all spectral regions, the

temporal evolutions of all (coupled) Gaussian amplitudes were fitted bi-exponentially in a global, least-squares fashion to yield the time constants $\tau_{solv} = 8.0 \pm 5.0$ ps and $\tau_{2AP} = 710 \pm 120$ ps in good agreement with our time-resolved emission measurements (3.0 ± 1.0 ps and 740 ± 15 ps).

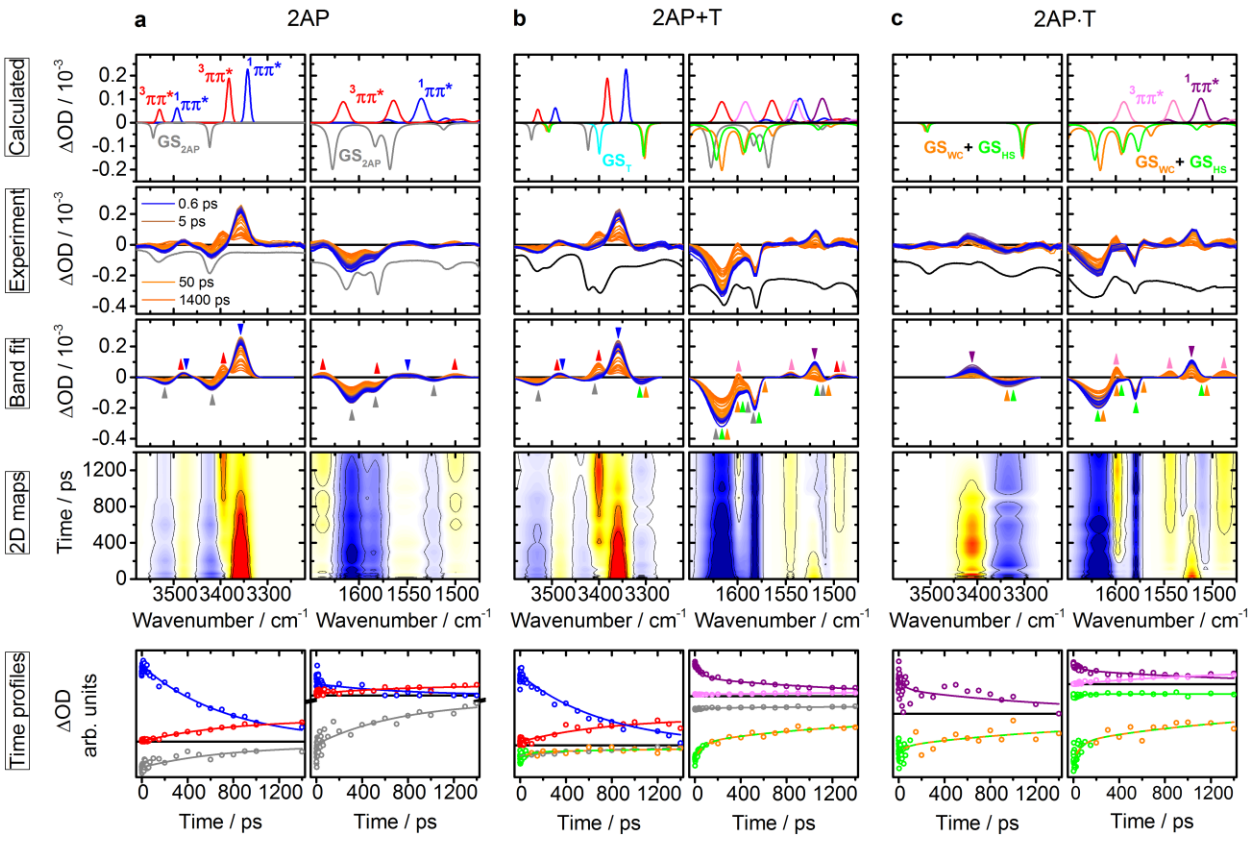

Figure 4. Transient vibrational absorption spectroscopic results. Comparison of the TVA spectra for free 2AP (2AP, a), a mixture of 2AP and T (2AP + T, b) and the difference of 2AP + T and 2AP to highlight pure dimer dynamics (2AP·T, c). **Calculated:** Computed ground-state vibrational spectra of free 2AP (grey), free T (cyan) and H-bonded 2AP·T in the Watson–Crick (WC, orange) and the Hoogsteen (HS, green) conformations as well as excited-state vibrational spectra in the $^1\pi\pi^*$ (2AP: blue, 2AP·T: purple) and $^3\pi\pi^*$ (2AP: red, 2AP·T: pink) states. **Experimental:** Time-resolved TVA spectra after 310 nm photoexcitation at selected pump–probe delay times (grey/black lines = inverse FTIR traces for reference). **Band fits:** Global Gaussian band fits to the experimental TVA spectra, with arrows indicating decaying and rising transient vibrational bands. **2D maps:** Spectro-temporal representations of the fitted data. Negative signals are shown in blue, red colours refer to positive TVA signals. **Time profiles:** Corresponding temporal evolutions of

Gaussian amplitudes of the global fit results to the TVA data and the associated result of an exponential global fit to the Gaussian amplitudes with up to four time constants (see text).

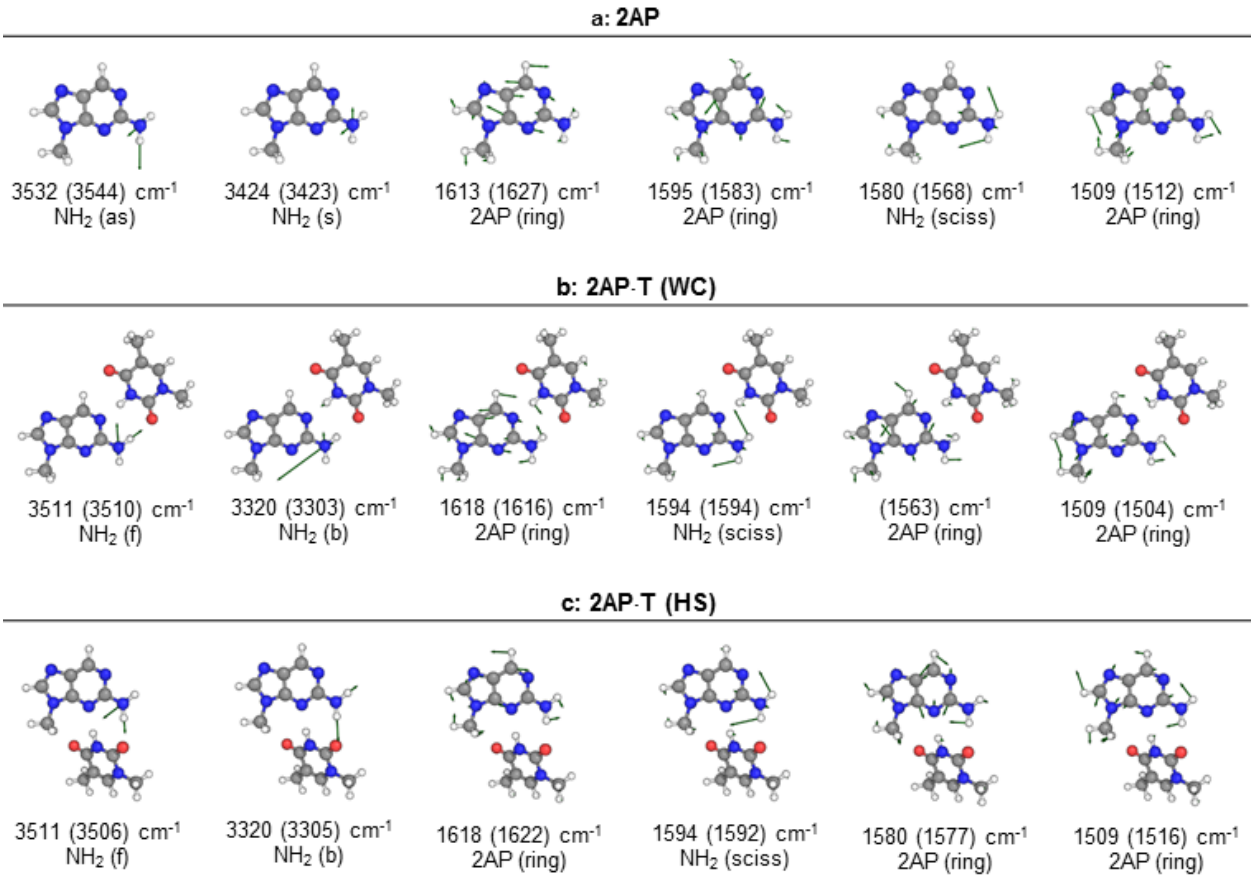

Figure 5. Computed vibrational ground-state modes of free 2AP and the 2AP·T dimers in the Watson–Crick and Hoogsteen conformations. Calculated ground-state vibrational marker bands of free 2AP (a) and the 2AP·T dimer in the Watson–Crick (WC, b) and Hoogsteen (HS, c) conformations. The experimental vibrational wavenumbers are from FTIR spectra and ground-state bleaching signals in the TVA spectra; the calculated wavenumbers are given in parentheses. The riboside residue in both chromophores was substituted by a methyl group in all calculations.

With these premises, we turn to the spectro-temporal evaluation of the 2AP+T mixture. Although many of the additional vibrational signatures in the TVA spectra after photoexcitation of the 2AP + T mixture (shown in Fig. 4b) are superimposed by transients of free 2AP, close inspection of the data readily reveals substantial contributions that have to be attributed to 2AP·T dimer species. Particular attention is directed at the features at 3309 cm^{-1}, 1620 – 1580 cm^{-1} and 1520 cm^{-1}. Here, the bleach at 3309 cm^{-1} observed after excitation of 2AP + T is absent in the TVA spectra of free 2AP (Fig. 4a). Also, the complex pattern around 1620 – 1580 cm^{-1} in the 2AP + T spectra is of very different shape and intensity than for 2AP. Additionally, the pronounced positive peak at 1520 cm^{-1} in the TVA spectra of 2AP + T is virtually absent in the spectra of free 2AP.

In order to highlight the identification of specific marker bands of 2AP·T species, Fig. 6 shows the global fit result of a sum of Gaussian functions to the TVA spectra of the 2AP+T mixture. Similar to data evaluation of free 2AP, the transient spectra in the region from 3600 – 3200 cm^{-1} are described by pairs for bleached ground-state recovery (grey), $^1\pi\pi^*$ decay (blue) and $^3\pi\pi^*$ formation (red) as marker bands for the antisymmetric and symmetric NH_2 stretching vibration in different electronic states of free 2AP. Notably, however, the TVA spectra feature an additional bleaching signal at 3309 cm^{-1}, in strikingly good agreement with our calculated bound NH_2 stretching vibration of 2AP·T species both in the WC (3303 cm^{-1}, orange) and HS (3305 cm^{-1}, green) conformation. Due to the strong overlap of these marker bands, the bleaching signal in the TVA data was modelled with a single Gaussian function. However, as further illustrated in Fig. 6, temporal evolution of this band proceeds in a bi-exponential manner within $\tau_{1,2AP\cdot T} \approx 70$ ps and $\tau_{2,2AP\cdot T} \approx 1.6$ ns. The same time constants, exclusive to 2AP·T species within the 2AP+T mixture,

have also been identified in the region of ring vibrations from 1650 – 1475 cm^{-1}. Due to strongly overlapping vibrational marker bands (cf. calculated vibrational spectra in Figs. 1, 4 and 5) in this spectral region, however, the transient spectra were modelled by a sum of eight Gaussian functions – four bleached signals at 1618 cm^{-1}, 1594 cm^{-1}, 1580 cm^{-1} and 1509 cm^{-1}, one Gaussian for $^1\pi\pi^*$ decay at 1519 cm^{-1} and three Gaussians for $^3\pi\pi^*$ formation at 1600 cm^{-1}, 1545 cm^{-1} and 1495 cm^{-1}. Evaluation of the temporal evolution of these bands (cf. Figs. 4 and 6) revealed kinetic contributions from both free 2AP and 2AP·T dimers. For instance, bleach-recovery of the TVA bands at 1618 (1627/1616/1622) cm^{-1}, 1594 (1583/1594/1592) cm^{-1} and 1509 (1512/1504/ 1516) cm^{-1} proceeds in a tri-exponential fashion within τ_{2AP}, $\tau_{1,2AP\cdot T}$ and $\tau_{2,2AP\cdot T}$ (calculated vibrations of free 2AP/WC/HS in parentheses, cf. Fig. 5). However, the bleached band at 1580 cm^{-1} is described by only bi-exponential recovery within τ_{2AP} and $\tau_{1,2AP\cdot T}$. Furthermore, in line with our time-resolved emission measurements, the marker band for the 2AP·T excited $^1\pi\pi^*$ state (purple) at 1519 cm^{-1} decays bi-exponentially within $\tau_{1,2AP\cdot T}$ and $\tau_{2,2AP\cdot T}$. Triplet formation (pink) at 1600 cm^{-1}, 1545 cm^{-1} and 1495 cm^{-1} proceeds mono-exponentially within $\tau_{2,2AP\cdot T}$, and is overlapped with contributions for $^3\pi\pi^*$ formation of free 2AP (red) only at 1495 cm^{-1} in agreement with our TVA measurements of free 2AP alone.

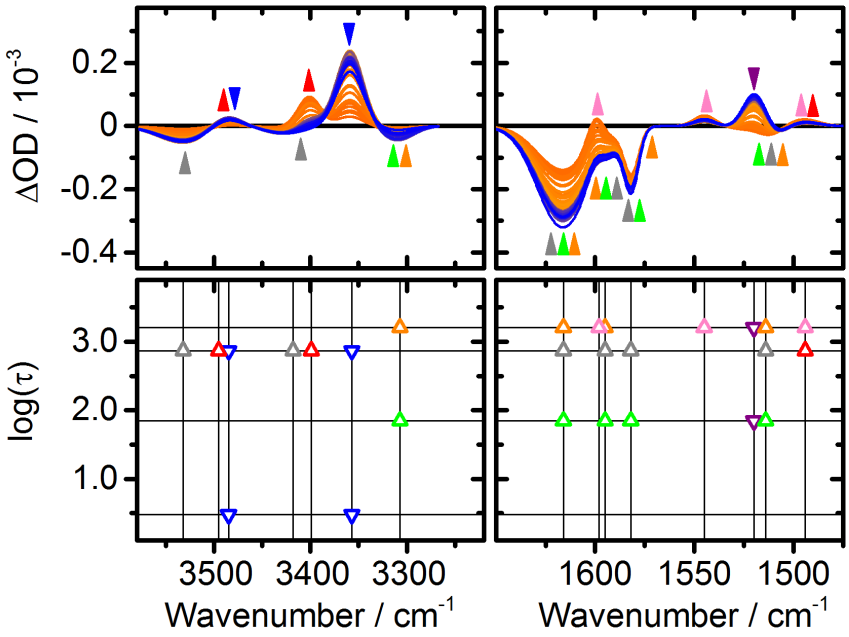

Figure 6. Two-dimensional spectro-temporal plot of TVA data. Vibrational marker bands for the 2AP + T mixture (cf. Fig 4b) are represented according to their associated wavenumbers and time constants. Free 2AP: Grey triangles represent ground-state recovery (GSR), $^{1}\pi\pi^{*}$ dynamics are shown in blue, red triangles indicate $^{3}\pi\pi^{*}$ formation. Dimeric 2AP·T: GSR is colour-coded as orange (Watson-Crick, WC) and green (Hoogsteen). Purple triangles refer to $^{1}\pi\pi^{*}$ dynamics of dimeric 2AP·T, pink triangles assign $^{3}\pi\pi^{*}$ formation of the WC pair.

In order to extract even minor contributions of 2AP·T dynamics superimposed by transient signals of free 2AP, the TVA spectra of free 2AP (Fig. 4a) were subtracted from the spectra recorded for the 2AP + T mixture (Fig. 4b). The isolated transient marker bands of 2AP·T dimers are displayed in Fig. 4c. As elaborated above, the excited state population of 2AP within the 2AP+T mixture is estimated to be ~ 50 %. As data acquisition was accomplished using doubled excitation energies for the 2AP+T mixture with respect to the monomer measurements (cf. Methods), no further scaling in the generation of 2AP·T spectra was applied. The resulting "pure"

transient vibrational 2AP·T spectra were subsequently modelled by a sum of two Gaussian functions in the NH_2 stretching region and a sum of eight Gaussians in the region of ring vibrations. Ground-state recovery of overlapping 2AP·T (WC/HS, orange/green) bleach signals at 3320 (3303/3305) cm^{-1}, 1618 (1616/1622) cm^{-1}, 1594 (1594/1592) cm^{-1} and 1509 (1504/ 1516) cm^{-1} unwinds bi-exponentially within $\tau_{1,2AP\cdot T}$ and $\tau_{2,2AP\cdot T}$. Notably, recovery of the bleached band at 1580 (1577) cm^{-1} is determined exclusively by the fast constant $\tau_{1,2AP\cdot T}$. Furthermore, excited $^1\pi\pi^*$ state (purple) vibrations at 3411 cm^{-1} and 1519 cm^{-1} decay in a bi-exponential manner within $\tau_{1,2AP\cdot T}$ and $\tau_{2,2AP\cdot T}$. Finally, $\tau_{2,2AP\cdot T}$ is found as the mono-exponential rising component in the marker bands of the $^3\pi\pi^*$ state (pink) at 1599 cm^{-1}, 1544 cm^{-1} and 1487 cm^{-1}.

Taking all spectral regions and time-resolved measurements into account, the encoded temporal information in our TVA data was extracted by a global least-squares fitting analysis of all time profiles (2AP, 2AP+T and 2AP·T) given in Fig. 4 in the bottom row using up to four exponentials to yield the time constants

$$\tau_{solv} = 3 \text{ ps (fixed)},$$

$$\tau_{2AP} = 740 \text{ ps (fixed)},$$

$$\tau_{1,2AP\cdot T} = 68 \pm 15 \text{ ps},$$

$$\tau_{2,2AP\cdot T} = 1.6 \pm 0.4 \text{ ns},$$

in satisfactory agreement with the time constants from the time-resolved fluorescence measurements above. The values for τ_{solv} and τ_{2AP} were fixed in this analysis at the above results for free 2AP, while $\tau_{1,2AP\cdot T}$ and $\tau_{2,2AP\cdot T}$ were taken as free-floating parameters. As opposed to the model-free analysis of our time-resolved fluorescence data, even the longest time constant $\tau_{2,2AP\cdot T}$ comes

out to be rather well determined by the coupling of related transient vibrational marker bands on the grounds of quantum chemical calculations, significantly stabilizing the fitting routine. Description of all time profiles in a global fit analysis further supports the reliability of time constants when compared to single individual time trace analyses. In the following, the distinct values of $\tau_{1,2AP\cdot T} \sim 70$ ps and $\tau_{2,2AP\cdot T} \sim 1.6$ ns will be attributed to the HS and WC conformations of 2AP·T.

DISCUSSION

The combined kinetic results from our time-resolved measurements are corroborated by the computed normal mode vibrations (cf. Fig. 5) that enable us to assign all observed vibrational bands and to interpret the entire spectro-temporal evolution encoded in our TVA spectra. In contrast to the antisymmetric and symmetric NH_2 modes of free 2AP, which are observed as distinct features in the electronic ground state at 3532 (3544) cm^{-1} and 3424 (3423) cm^{-1} (calculated values in parentheses), the corresponding vibrational modes associated with the 2AP·T dimers, observed at 3511 and 3320 cm^{-1}, are subject to spectral broadening caused by H-bonding and overlapping bands of both the WC (calculated at 3510 and 3303 cm^{-1}) and HS (3506 and 3305 cm^{-1}) conformations. While the bleach signals of the free (f) NH_2 stretching modes of 2AP·T (WC and HS) at 3511 cm^{-1} are too weak to be detected in the transient spectra, the corresponding vibrations in the $^1\pi\pi^*$ excited state show up as positive absorptions at 3411 cm^{-1} directly after excitation and decay in a bi-exponential manner with $\tau_{1,2AP\cdot T}$ and $\tau_{2,2AP\cdot T}$. Accordingly, this band is assumed to be a superposition of the WC and HS conformations. It follows the trend for a red-shift of the absorption in the $^1\pi\pi^*$ state relative to the GS as also found for free 2AP. Likewise, the

bleached 2AP·T band at 3320 cm^{-1} arises from the superimposed bound (b) NH_2 stretching vibrations of 2AP·T in the WC (3303 cm^{-1}) and HS (3305 cm^{-1}) conformations. Recovery to the GS of this superimposed band proceeds bi-exponentially with $\tau_{1,2AP\cdot T}$ and $\tau_{2,2AP\cdot T}$. The associated $^1\pi\pi^*$ excited-state vibration is expected to be red-shifted in absorption and to have moved out of the detection window in Fig. 4. Another characteristic absorption associated with the $^1\pi\pi^*$ state is present at 1519 cm^{-1} in the region of the ring vibrations directly after excitation, which also decays in a bi-exponential manner with $\tau_{1,2AP\cdot T}$ and $\tau_{2,2AP\cdot T}$. The bi-exponential decay of the $^1\pi\pi^*$ state with $\tau_{1,2AP\cdot T}$ and $\tau_{2,2AP\cdot T}$ is in good agreement with the results of the time-resolved fluorescence experiments, thus the fast picosecond time constant components obtained in the fluorescence (44 ± 10 ps) and vibrational absorption (68 ± 15 ps) experiments are considered to arise from the same species within the error limits. Further, the overlapping 2AP·T(WC/HS) bleach signals at 1618 (1616/1622) cm^{-1}, 1594 (1594/1592) cm^{-1} and 1509 (1504/1516) cm^{-1} recover bi-exponentially with $\tau_{1,2AP\cdot T}$ and $\tau_{2,2AP\cdot T}$ as well. Most importantly, however, the recovery of the characteristic bleached band at 1580 (1577) cm^{-1} is determined by the fast $\tau_{1,2AP\cdot T}$ = 68 ps time constant only. Based on the specifics of the electronic relaxation pathways (see below), we attribute this band to H-bonded 2AP·T in the HS conformation. In fact, the association with a specific 2AP·T conformation of this rather well-separated vibrational marker band at 1580 (1577) cm^{-1} along with its domination by $\tau_{1,2AP\cdot T}$ led us to attribute the fast time constant $\tau_{1,2AP\cdot T}$ to the electronic deactivation of the $^1\pi\pi^*$ state of the HS conformation of 2AP·T, and, vice versa, the slow time constant $\tau_{2,2AP\cdot T}$ to the deactivation of the $^1\pi\pi^*$ state of 2AP·T in the WC conformation.

Combining the information from our time-resolved fluorescence and vibrational absorption measurements, we propose the overall scheme for the electronic relaxation dynamics of 2AP·T in

the WC and HS conformations sketched in Fig. 7: After UV excitation of the 2AP moiety in the 2AP·T(WC) base pair, the molecule rapidly relaxes from the initial FC geometry to the $^1\pi\pi^*$ potential energy minimum. According to our excited-state calculations, the structure of the 2AP moiety in the WC dimer resembles the $^1\pi\pi^*$ minimum energy structure of free 2AP to a high extent. The rather flat structure of the WC dimer is slightly broken by the six-membered ring puckering at the C^6 position of the 2AP chromophore similar to free 2AP.[62] Thus, H-bonding of the 2AP moiety with T in the WC conformation exerts little effect on the structure of the 2AP chromophore in the $^1\pi\pi^*$ excited state. The energies of the different electronic states, on the other hand, and their crossings are more strongly affected. As has recently been shown,[14] the $^1\pi\pi^*$ lifetime of 2AP is significantly increased upon H-bonding due to an increased energy of the $^1n\pi^*$ state and the associated $^1\pi\pi^*/^1n\pi^*$ conical intersection. Congruently, we observe the increased fluorescence lifetime of the 2AP moiety by H-bonding with T in the WC motif to $\tau_{2AP\cdot T(WC)} = 1.6$ ns, substantially longer than the lifetime of free 2AP ($\tau_{2AP} = 740$ ps). Due to the structural similarity, however, the ensuing dynamics of 2AP·T(WC) are expected to follow similar pathways as in free 2AP. Hence, we expect transient population of a short-lived $^1n\pi^*$ state that acts as an intermediate state for both efficient GS recovery and $^3\pi\pi^*$ formation. In line with these considerations, we observe the 1.6 ns time constant in the ground-state recovery time profiles of the bleaching signals at 3320 cm^{-1}, 1618 cm^{-1}, 1594 cm^{-1}, 1509 cm^{-1}, and as the rising component in the marker bands of the $^3\pi\pi^*$ state at 1599 cm^{-1}, 1544 cm^{-1} and 1487 cm^{-1}. The experimentally observed vibrational bands associated with 2AP·T(WC) in the $^3\pi\pi^*$ state coincide strikingly well with the frequency-shifted calculated spectrum for the triplet vibrations of free 2AP in the region of the ring vibrations, again highlighting the similarity between free 2AP and the 2AP moiety in the 2AP·T(WC) base pair.

In contrast to 2AP·T(WC), the structure of the 2AP moiety in the HS network in the excited $^1\pi\pi^*$ state gets more strongly distorted by H-bonding with T. According to our excited-state calculations as shown in Fig. 7, partial planarity of the 2AP moiety in the 2AP·T(HS) conformation is maintained due to the effect of inter-base H-bonding. At the same time, however, the steric influence of the bulky residue at the 9-position in 2AP pushes the chromophore away from planarity. As a result, the 2AP moiety in the HS 2AP·T conformation appears to be bent along the C^6/N^3 axis in the $^1\pi\pi^*$ state. According to our time-resolved experiments, this distorted species finds an efficient route for electronic de-excitation to the GS in ~ 68 ps ($\tau_{2AP\cdot T(HS)}$). Interestingly, this time constant contributes to the decay of the bright $^1\pi\pi^*$ and to the recovery of the GS vibrations of 2AP·T(HS), but not as a rising component in triplet formation. Hence, we attribute $\tau_{2AP\cdot T(HS)}$ to direct repopulation of the electronic ground state from the initially excited $^1\pi\pi^*$ state.

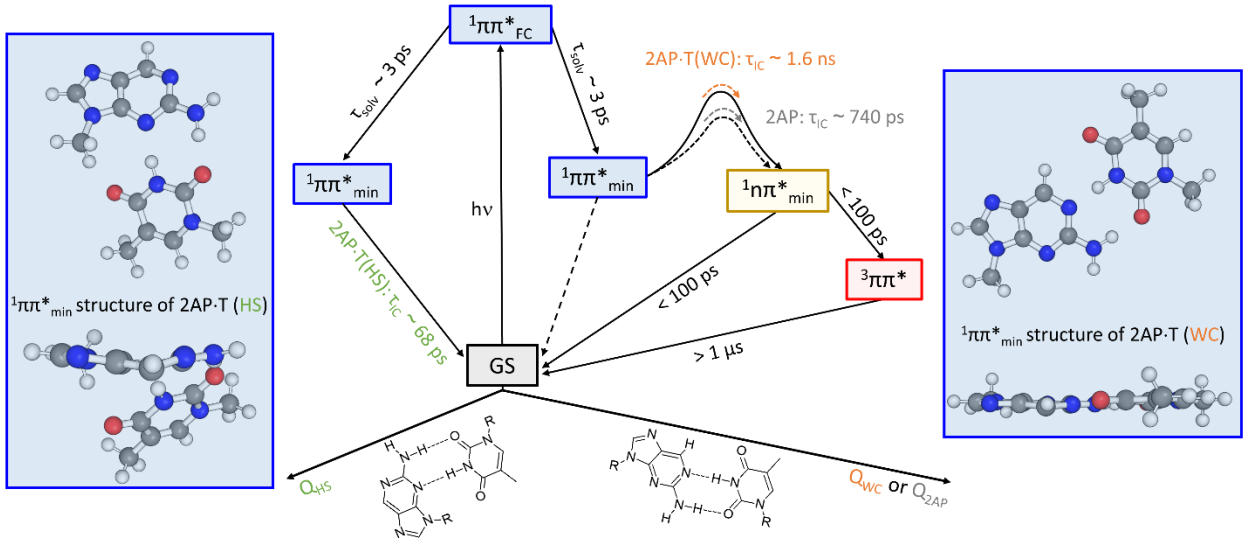

Figure 7. Schematic depiction of the proposed electronic deactivation pathways after UV excitation for free 2AP, 2AP·T in the Watson–Crick (WC) and 2AP·T in the Hoogsteen (HS)

conformations. The excited-state $S_1(^1\pi\pi^*)$ minimum structures of 2AP·T in the WC (right) and HS (left) conformations were calculated at the RI-CC2/def2-SVP level of theory.

Exploring deactivation pathways of 2AP·T in the Hoogsteen conformation

Since our chemical structure and electronic state-sensitive time-resolved results enabled us to distinguish between the distinct deactivation dynamics of 2AP·T in the WC and HS forms, the focus moves to the reason for the much faster electronic deactivation in the HS configuration. Here, the possibility of excited-state proton transfer has lately gained much attention as an efficient way for electronic deactivation in H-bonded nucleobases. For example, excited-state proton transfer accounts for highly efficient electronic deactivation in the G·C Watson–Crick base pair,[35,68] while no comparable evidence for such a process was found for the A·T pair in the Watson–Crick conformation.[69] To explore the possibility of excited-state proton transfer in the 2AP·T base pair forms, Fig. 8 maps the energies of various electronic states along an extended N–H distance in the 2AP moiety of 2AP·T. Starting from the ground-state minimum structure, Fig. 8 maps the electronic energy of the GS (RI-MP2/def2-SVP) at extended, frozen N–H distances. For all calculations, only the N–H bond distance of 2AP was frozen at discrete values, while all other degrees of freedom were allowed to relax unrestrictedly. As illustrated by insets in Fig. 8, elongation of the N–H distance results in single proton transfer (SPT) from 2AP to T followed by spontaneous transfer of the central inter-molecularly bonded proton from T to 2AP (double proton transfer, DPT) both in the electronic GS and excited $^1\pi\pi^*$ state of 2AP·T in both the WC and HS conformation. In the electronic ground state (black solid circles), however, this process is associated with a sizable energy barrier. Also, as the DPT species is rendered unstable, DPT is not expected in the GS on the grounds of our calculations. For every optimized ground-state structure,

the energies of higher excited states upon vertical excitation are plotted in coloured open circles. No crossing of excited states, nor the occasion of charge transfer states could be observed along the N–H bond distance coordinate for 2AP·T in the WC and HS forms.

Analogous restricted excited-state geometry optimizations in the first excited $^1\pi\pi^*$ state at extended N–H distances have been performed at the RI-ADC(2)/def2-SVP level of theory as shown as solid blue squares in Fig. 8. Accordingly, spawning from the Franck-Condon region on the excited $^1\pi\pi^*$ potential surface, excited-state PT is associated with a moderate energy barrier. As opposed to the GS, however, the DP-transferred species is expected to be stable in the excited $^1\pi\pi^*$ state according to our calculations. Hence, excited-state DPT is possible for 2AP·T in both the WC and HS motifs. Yet, the rather flat potential energy surface would probably impede the occurrence of distinct vibrational marker bands in our TVA spectra. Most importantly, however, Fig. 8 additionally maps the potential energy of the GS (open squares) corresponding to relaxed excited-state structures. Accordingly, the potential energy of the GS is dramatically affected by excited-state DPT in the HS form.

Hence, in line with recent findings on the grounds of quantum chemical calculations,[70] excited-state proton transfer is not expected as an efficient way for electronic deactivation within the WC conformation of 2AP·T. Surprisingly, however, our calculations predict a conical intersection as an efficient electronic de-excitation pathway in the HS conformation that connects the $^1\pi\pi^*$ state with the electronic GS at a double proton-transferred species after overcoming a small potential energy barrier induced by single proton transfer. Following the scenario sketched in Fig. 8, the excited-state HS population is expected to evolve to the GS, once the excited-state barrier is overcome, while the WC form features no such deactivation pathways. Back in the GS, the original HS conformation likely recovers, as the proton-transferred species is unstable in the GS. At this

point, we emphasize that efficient electronic deactivation along a double proton transfer coordinate followed by recovery of the original HS species in the GS is consistent with our time-resolved measurements. Still, highly efficient electronic deactivation to the GS within $\tau_{HS} \sim 68$ ps may be possible, in principle, along other coordinates. In fact, given the highly bent structure of the HS form in the excited $^1\pi\pi^*$ state, chemical intuition suggests a conical intersection along a ring-puckered mode in close vicinity to the excited-state minimum structure. Thus, more elaborate quantum chemical calculations are desirable to elucidate the pathways for electronic deactivation in the 2AP·T(HS) dimer.

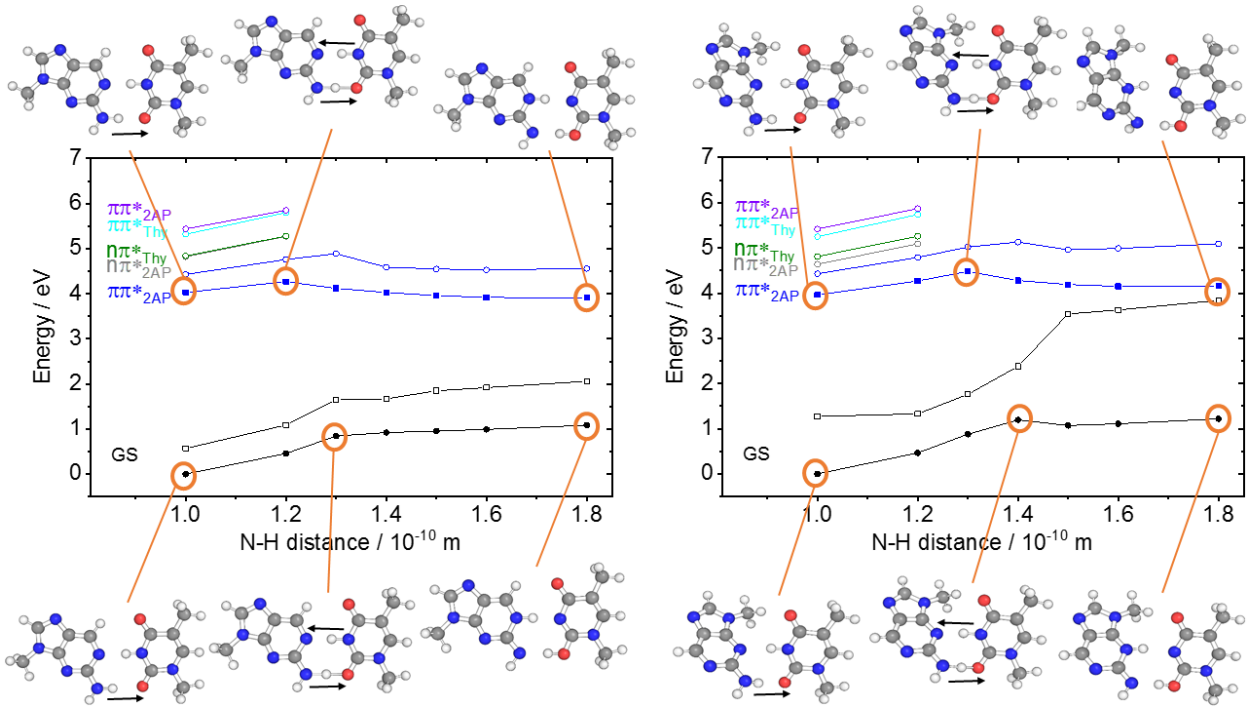

Figure 8. Potential energy curves along the proton-transfer coordinate for 2AP·T in the Watson–Crick (WC, left) and Hoogsteen (HS, right) conformations. Open circles represent vertical RI-ADC(2)/def2-SVP energies relative to restricted RI-MP2/def2-SVP ground-state optimizations (solid black circles). Squares indicate the respective energies relative to restricted S_1 excited-state RI-ADC(2)/def2-SVP optimizations. Virtually the same results were found for rWC and rHS conformations.

CONCLUSIONS

We have investigated distinct electronic relaxation pathways in H-bonded 2AP·T dimers in the Watson–Crick (WC) and Hoogsteen (HS) conformations after UV photoexcitation, by time-resolved fluorescence and transient vibrational absorption spectroscopy methods aided by quantum chemical calculations. When compared to free 2AP, H-bonding with T exerts little effect on the structure of the 2AP chromophore in the WC form. Hence, similar to free 2AP, electronic deactivation of the initially excited $^1\pi\pi^*$ state proceeds to a short-lived intermediate state of $^1n\pi^*$ character, followed partially by recovery of the electronic ground state and partially by crossing to the $^3\pi\pi^*$ state. However, the energetic barrier for the internal conversion to the $^1n\pi^*$ state is raised by the H-bonding in 2AP·T(WC). Thus, the $^1\pi\pi^*$ lifetime is increased from τ_{2AP} = 740 ps to $\tau_{2AP\cdot T(WC)} \sim 1.6$ ns. In contrast, the structure of the 2AP moiety in the HS base pair is distorted in the $^1\pi\pi^*$ excited state. The distorted structure opens up new pathways for electronic deactivation. In particular, direct recovery is observed from the initially excited $^1\pi\pi^*$ state to the electronic ground state in $\tau_{2AP\cdot T(HS)} \sim 68$ ps. Although other electronic de-excitation coordinates cannot be ruled out, the observed dynamics are in accordance with a calculated double-proton transfer process in the photoexcited $^1\pi\pi^*$ state of the 2AP·T(HS) base pair. As most of the vibrational marker bands for 2AP·T in the Watson–Crick and Hoogsteen conformations overlap and the relative ratio of both conformations can only be estimated to be roughly the same, statements about quantum yields remain tentative. Still, as the fast time constant $\tau_{HS} \sim 68$ ps is not found as a rising component in the marker bands associated with the $^3\pi\pi^*$ state, we conclude that the significant contribution to triplet formation stems from 2AP·T in the Watson-Crick conformation with a quantum yield similar to that in free 2AP (i.e., ~ 42%).

Commonly, 2AP is used as an intrinsic fluorescent probe to report on conformational motifs in duplex DNA. Typically, 2AP-containing DNA duplexes feature fluorescence decay times of $\tau_1 < 100$ ps, $\tau_2 \sim 0.5$ ns, $\tau_3 \sim 2$ ns and $\tau_4 \sim 10$ ns. Quenching of excited-state lifetimes is widely attributed to charge transfer and intra-strand stacking interactions. However, we note that τ_1 and τ_3 coincide strikingly well with our $\tau_{2AP\cdot T(HS)}$ and $\tau_{2AP\cdot T(WC)}$ values, respectively, obtained from study of the dynamics of purely H-bonded 2AP·T dimers. As recent research highlights the abundance of transient HS motifs in duplex DNA, our results suggest extending the established picture for dynamic fluorescence quenching of 2AP by also incorporating dynamic inter-strand H-bonding effects.

ASSOCIATED CONTENT

Supporting Information

The following files are available free of charge.

Calculated vertical excitation energies for free 2AP, 2AP·T_{WC} and 2AP·T_{HS}. (PDF)

AUTHOR INFORMATION

Corresponding Authors

*E-mail: temps@phc.uni-kiel.de

*E-mail: A.Orr-Ewing@bristol.ac.uk

Notes

The authors declare no competing financial interests.

ACKNOWLEDGMENT

The laser system and research at the University of Bristol were supported by ERC Advanced Grant CAPRI 290966. The group at the University of Kiel has been supported by the Deutsche Forschungsgemeinschaft through the Collaborative Research Centre 677 “Function by Switching”. KR received support by the DFG grant RO 4952/1-1. HJBM and RAI were supported by EPSRC Doctoral Training Grant awards.

REFERENCES

(1) Ward, D. C.; Reich, E.; Stryer, L. Fluorescence Studies of Nucleotides and Polynucleotides. *J. Biol. Chem*. **1969**, *244*, 1228–1237.

(2) Guest, C. R.; Hochstrasser, R. A.; Sowers, L. C.; Millar, D. P. Dynamics of Mismatched Base Pairs in DNA. *Biochemistry* **1991**, *30*, 3271–3279.

(3) Kawai, M.; Lee, M. J.; Evans, K. O.; Nordlund, T. M. Temperature and Base Sequence Dependence of 2-Aminopurine Fluorescence Bands in Single- and Double-Stranded Oligodeoxynucleotides. *J. Fluoresc*. **2001**, *11*, 23–32.

(4) Sowers, L. C.; Fazakerleyt, G. V.; Eritjat, R.; Kaplant, B. E.; Goodman, M. F.; Benson, S. W. Base Pairing and Mutagenesis: Observation of a Protonated Base Pair between 2-Aminopurine and Cytosine in an Oligonucleotide by Proton NMR. *Proc. Natl. Acad. Sci. U.S.A* **1986**, *83*, 5434–5438.

(5) Nordlund, T. M.; Andersson, S.; Nilsson, L.; Rigler, R.; Gráslund, A.; Mclaughlin, L. W. Structure and Dynamics of a Fluorescent DNA Oligomer Containing the EcoRI Recognition Sequence: Fluorescence, Molecular Dynamics, and NMR Studies. *Biochemistry* **1989**, *28*, 9095–9103.

(6) Johnson, N. P.; Baase, W. A.; von Hippel, P. H. Low-Energy Circular Dichroism of 2-Aminopurine Dinucleotide as Probe of Local Conformation of DNA and RNA. *Proc. Natl. Acad. Sci. U.S.A* **2004**, *101*, 3426–3431.

(7) Dallmann, A.; Dehmel, L.; Peters, T.; Mügge, C.; Griesinger, C.; Tuma, J.; Ernsting, N. 2-Aminopurine Incorporation Perturbs the Dynamics and Structure of DNA. *Angew. Chem. Int. Ed.* **2010**, *49*, 5989–5992.

(8) Rachofsky, E.; Osman, R.; Ross, J. Probing Structure and Dynamics of DNA with 2-Aminopurine: Effects of Local Environment on Fluorescence. *Biochemistry* **2001**, *40*, 946–956.

(9) Pal, S. K.; Zhao, L.; Xia, T.; Zewail, A. H. Site- and Sequence-Selective Ultrafast Hydration of DNA. *Proc. Natl. Acad. Sci. U.S.A* **2003**, *100*, 13746–13751.

(10) Neely, R. K.; Megennis, S. W.; Dryden, D. T. S.; Jones, A. C. Evidence of Tautomerism in 2-Aminopurine from Fluorescence Lifetime Measurements. *J. Phys. Chem. B* **2004**, *108*, 17606–17610.

(11) Somsen, O. J. G.; van Hoek, A.; van Amerongen, H. Fluorescence Quenching of 2-Aminopurine in Dinucleotides. *Chem. Phys. Lett.* **2005**, *402*, 61–65.

(12) Gelot, T.; Tourón-Touceda, P.; Crégut, O.; Léonard, J.; Haacke, S. Ultrafast Site-Specific Fluorescence Quenching of 2-Aminopurine in a DNA Hairpin Studied by Femtosecond Down-Conversion. *J. Phys. Chem. A* **2012**, *116*, 2819–2825.

(13) Jones, A. C.; Neely, R. K. 2-Aminopurine as a Fluorescent Probe of DNA Conformation and the DNA–Enzyme Interface. *Quart. Rev. Biophys*. **2015**, *48*, 244–279.

(14) Lobsiger, S.; Blaser, S.; Sinha, R. K.; Frey, H.-M.; Leutwyler, S. Switching on the Fluorescence of 2-Aminopurine by Site-Selective Microhydration. *Nat. Chem*. **2014**, *6*, 989–993.

(15) Barbatti, M.; Lischka, H. Why Water Makes 2-Aminopurine Fluorescent? *Phys. Chem. Chem. Phys*. **2015**, *17*, 15452–15459.

(16) Neely, R. K.; Jones, A. C. Influence of Base Pairing Dynamics on the Conformational Properties of DNA: Observation of Static Conformational States in Rigid Duplexes at 77 K. *J. Am. Chem. Soc.* **2006**, *128*, 15952–15953.

(17) Degtyareva, N. N.; Reddish, M. J.; Sengupta, B.; Petty, J. T. Structural Study of a Trinucleotide Repeat Sequence using 2-Aminopurine. *Biochemistry* **2009**, *48*, 2340–2346.

(18) Jean, J. M.; Hall, K. B. 2-Aminopurine Fluorescence Quenching and Lifetimes: Role of Base Stacking. *Proc. Natl. Acad. Sci.* **2001**, *98*, 37–41.

(19) Jean, J. M.; Krueger, B. P. Structural Fluctuations and Excitation Transfer between Adenine and 2-Aminopurine in Single-Stranded Deoxytrinucleotides. *J. Phys. Chem. B* **2006**, *110*, 2899–2909.

(20) Bonnist, E. Y. M.; Jones, A. C. Long-Wavelength Fluorescence from 2-Aminopurine-Nucleobase Dimers in DNA. *ChemPhysChem* **2008**, *9*, 1121–1129.

(21) Hariharan, C.; Bloom, L. B.; Helquist, S. A.; Kool, E. T.; Reha-Kranz, L. J. Dynamics of Nucleotide Incorporation: Snapshots Revealed by 2-Aminopurine Fluorescence Studies. *Biochemistry* **2006**, *45*, 2836–2844.

(22) Kelley, S.; Barton, J. Electron Transfer between Bases in Double Helical DNA. *Science* **1999**, *283*, 375–380.

(23) Genereux, J.; Wuerth, S.; Barton, J. Single-Step Charge Transport through DNA over Long Distances. *J. Am. Chem. Soc*. **2011**, *133*, 3863–3868.

(24) Genereux, J.; Barton, J. Mechanisms for DNA Charge Transport. *Chem. Rev*. **2010**, *10*, 1642–1662.

(25) Crespo-Hernández, C. E.; Cohen, B.; Hare, P. M.; Kohler, B. Ultrafast Excited-State Dynamics in Nucleic Acids. *Chem. Rev*. **2004**, *104*, 1977–2019.

(26) Schwalb, N. K.; Temps, F. Base Sequence and Higher-Order Structure Induce the Complex Excited-State Dynamics in DNA. *Science* **2008**, *322*, 243–245.

(27) Middleton, C. T.; de La Harpe, K.; Su, C.; Law, Y. K.; Crespo-Hernández, C. E.; Kohler, B. DNA Excited-State Dynamics: From Single Bases to the Double Helix. *Annu. Rev. Phys. Chem.* **2009**, *60*, 217–239.

(28) Spata, V. A.; Lee, W.; Matsika, S. Excimers and Exciplexes in Photoinitiated Processes of Oligonucleotides. *J. Phys. Chem. Lett*. **2016**, *7*, 976–984.

(29) Schreier, W. J.; Gilch, P.; Zinth, W. Early Events of DNA Photodamage. *Annu. Rev. Phys. Chem.* **2015**, *66*, 497–519.

(30) Marquetand, P.; Nogueira, J.; Mai, S.; Plasser, F.; González, L. Challenges in Simulating Light-Induced Processes in DNA. *Molecules* **2016**, *49*, 1–22.

(31) Nikolova, E. N.; Kim, E.; Wise, A. A.; O'Brien, P. J.; Andricioaei, I.; Al-Hashimi, H. M. Transient Hoogsteen Base Pairs in Canonical Duplex DNA. *Nature* **2011**, *470*, 498–502.

(32) Chakraborty, D.; Wales, D. J. Energy Landscape and Pathways for Transitions between Watson–Crick and Hoogsteen Base Pairing in DNA. *J. Phys. Chem. Lett*. **2018**, *9*, 229–241.

(33) Siriwong, K.; Voityuk, A.; Newton, M.; Rösch, N. Estimate of the Reorganization Energy for Charge Transfer in DNA. *J. Phys. Chem. B* **2003**, *107*, 2595–2601.

(34) Roberts, G. M.; Marroux, H. J. B.; Grubb, M. P.; Ashfold, M. N. R.; Orr-Ewing, A. J. On the Participation of Photoinduced N–H Bond Fission in Aqueous Adenine at 266 and 220 nm: A Combined Ultrafast Transient Electronic and Vibrational Absorption Spectroscopy Study. *J. Phys. Chem. A* **2014**, *118*, 11211–11225.

(35) Schwalb, N. K.; Temps, F. Ultrafast Electronic Relaxation in Guanosine is Promoted by Hydrogen Bonding with Cytidine. *J. Am. Chem. Soc*. **2007**, *129*, 9272–9273.

(36) Zhao, Y.; Truhlar, D. G. The M06 Suite of Density Functionals for Main Group Thermochemistry, Thermochemical Kinetics, Noncovalent Interactions, Excited States, and Transition Elements: Two New Functionals and Systematic Testing of Four M06-class Functionals and 12 Other Functionals. *Theor. Chem. Acc*. **2008**, *120*, 215–241.

(37) McLean, A. D.; Chandler, G. S. Contracted Gaussian Basis Sets for Molecular Calculations. I. Second Row Atoms, Z =11–18. *J. Chem. Phys*. **1980**, *72*, 5639–5648.

(38) Krishnan, J. S.; Binkley, J. S.; Seeger, R.; Pople, J. A. Self-Consistent Molecular Orbital Methods. XX. A Basis Set for Correlated Wave Functions. *J. Chem. Phys*. **1980**, *72*, 650–654.

(39) Frisch, M. J.; Pople, J. A.; Binkley, J. S. Self-Consistent Molecular Orbital Methods 25. Supplementary Functions for Gaussian Basis Sets. *J. Chem. Phys*. **1984**, *80*, 3265–3269.

(40) Clark, T.; Chandrasekhar, J.; Spitznage, G. W.; von Ragué Schleyer, P. Efficient Diffuse Function-Augmented Basis Sets for Anion Calculations. III. The 3-21+G Basis Set for First-Row Elements, Li–F. *J. Comput. Chem*. **1983**, *4*, 294–300.

(41) Frisch, M. J.; Trucks, G. W.; Schlegel, H. B.; Scuseria, G. E.; Robb, M. A.; Cheeseman, J. R.; Scalmani, G.; Barone, V.; Mennucci, B.; Petersson, G. A.; et al. (Gaussian 09, Revision D.01). Wallingford CT. **2013**.

(42) Laury, M. L.; Boesch, S. E.; Haken, I.; Sinha, P.; Wheeler, R. A.; Wilson, A. K. Harmonic Vibrational Frequencies: Scale Factors for Pure, Hybrid, Hybrid Meta, and Double-Hybrid Functionals in Conjunction with Correlation Consistent Basis Sets. *J. Comput. Chem*. **2011**, *32*, 2339–2347.

(43) Laury, M. L.; Carlson, M. J.; Wilson, A. K. Vibrational Frequency Scale Factors for Density Functional Theory and the Polarization Consistent Basis Sets. *J. Comput. Chem*. **2012**, *33*, 2380–2387.

(44) Grimme, S. Semiempirical Hybrid Density Functional with Perturbative Second-Order Correlation. *J. Chem. Phys*. **2006**, 124, 034108.

(45) Weigend, F.; Furche, F.; Ahlrichs, R. Gaussian Basis Sets of Quadruple Zeta Valence Quality for Atoms H–Kr. *J. Chem. Phys*. **2003**, *119*, 12753–12762.

(46) TURBOMOLE V7.0 2015, a Development of University of Karlsruhe and Forschungszentrum Karlsruhe GmbH, 1989-2015, TURBOMOLE GmbH, since **2007**; Available from http://www.turbomole.com.

(47) Schwabe, T.; Grimme, S. Double-Hybrid Density Functionals with Long-Range Dispersion Corrections: Higher Accuracy and Extended Applicability. *Phys. Chem. Chem. Phys*. **2007**, 9, 3397–3406.

(48) Goerigk, L.; Kruse, H.; Grimme, S. Benchmarking Density Functional Methods against the S66 and S66x8 Datasets for Non-Covalent Interactions. *ChemPhysChem* **2011**, *12*, 3421–3433.

(49) Häser, M.; Ahlrichs, R. Improvements on the Direct SCF Method. *J. Comput. Chem.* **1989**, *10*, 104–111.

(50) Weigend, F.; Häser, M. RI-MP2: First Derivatives and Global Consistency. *Theor. Chem. Acc.* **1997**, *97*, 331–340.

(51) Weigend, F.; Häser, M.; Patzelt, H.; Ahlrichs, R. RI-MP2: Optimized Auxiliary Basis Sets and Demonstration of Efficiency. *Chem. Phys. Lett.* **1998**, *294*, 143–152.

(52) Hättig, C.; Hellweg, A.; Köhn, A. Distributed Memory Parallel Implementation of Energies and Gradients for Second-Order Møller-Plesset Perturbation Theory with the Resolution-of-the-Identity Approximation. *Phys. Chem. Chem. Phys.* **2006**, *8*, 1159–1169.

(53) Schäfer, A.; Horn, H.; Ahlrichs, R. Fully Optimized Contracted Gaussian Basis Sets for Atoms Li to Kr. *J. Chem. Phys*. **1992**, *97*, 2571–2577.

(54) Weigend, F.; Ahlrichs, R. Balanced Basis Set of Split Valence, Triple Zeta Valence and Quadruple Zeta Valence Quality for H to Rn: Design and Assessment of Accuracy. *Phys. Chem. Chem. Phys.* **2005**, *7*, 3297–3305.

(55) Rappoport, D.; Furche, F. Property-Optimized Gaussian Basis Sets for Molecular Response Calculations. *J. Chem. Phys.* **2010**, *133*, 134105.

(56) Hellweg, A.; Grün, S. A.; Hättig, C. Benchmarking the Performance of Spin-Component Scaled CC2 in Ground and Electronically Excited States. *Phys. Chem. Chem. Phys.* **2008**, *10*, 4119–4127.

(57) Ahlrichs, R. Efficient Evaluation of Three-Center Two-Electron Integrals over Gaussian Functions. *Phys. Chem. Chem. Phys.* **2004**, *6*, 5119–5121.

(58) Hättig, C.; Köhn, A. Transition Moments and Excited-State First-Order Properties in the Coupled-Cluster Model CC2 using the Resolution-of-the-Identity Approximation. J. *Chem. Phys.* **2002**, *117*, 6939–6951.

(59) Köhn, A.; Hättig, C. Analytic Gradients for Excited States in the Coupled-Cluster Model CC2 Employing the Resolution-of-the-Identity Approximation. *J. Chem. Phys.* **2003**, *119*, 5021–5036.

(60) Hättig, C.; Weigend, F. CC2 Excitation Energy Calculations on Large Molecules using the Resolution of the Identity Approximation. *J. Chem. Phys.* **2000**, *113*, 5154–5161.

(61) Christiansen, O.; Koch, H.; Jørgensen, P. The Second-Order Approximate Coupled Cluster Singles and Doubles Model CC2. *Chem. Phys. Lett.* **1995**, *243*, 409–418.

(62) Böhnke, H.; Röttger, K.; Ingle, R. A.; Marroux, H. J. B.; Bohnsack, M.; Orr-Ewing, A. J.; Temps, F. Efficient Intersystem Crossing in 2-Aminopurine Riboside Probed by Femtosecond Time-Resolved Transient Vibrational Absorption Spectroscopy. *Phys. Chem. Chem. Phys.* **2018**, *20*, 20033–20042.

(63) Friese, D. H.; Törk, L.; Hättig, C. Vibrational Frequency Scaling Factors for Correlation Consistent Basis Sets and the Methods CC2 and MP2 and their Spin-Scaled SCS and SOS Variants. *J. Chem. Phys*. **2014**, *141*, 194106.

(64) Schirmer, J. Beyond the Random-Phase Approximation: A New Approximation Scheme for the Polarization Propagator. *Phys. Rev. A*. **1982**, *26*, 2395–2416.

(65) Röttger, K.; Marroux, H. J. B.; Böhnke, H.; Morris, D. T. J.; Voice, A. T.; Temps, F.; Roberts, G. M.; Orr-Ewing, A. J. Probing the Excited State Relaxation Dynamics of Pyrimidine Nucleosides in Chloroform Solution. *Faraday Discuss*. **2016**, *194*, 683–708.

(66) Brovarets, O. O.; Pérez-Sánchez, H.; Hovorun, D. M. Structural Grounds for the 2-Aminopurine Mutagenicity: A Novel Insight into the Old Problem of the Replication Errors. *RSC Adv*. **2016**, *6*, 99546–99557.

(67) Reichardt, C.; Wen, C.; Vogt, R. A.; Crespo-Hernández, C. E. Role of Intersystem Crossing in the Fluorescence Quenching of 2-Aminopurine 2-Deoxyriboside in Solution. *Photochem. Photobiol. Sci.* **2013**, *12*, 1341–1350.

(68) Röttger, K.; Marroux, H. J. B.; Grubb, M. P.; Coulter, P. M.; Böhnke, H.; Henderson, A. S.; Galan, M. C.; Temps, F.; Orr-Ewing, A. J.; Roberts, G. M. Ultraviolet Absorption

Induces Hydrogen-Atom Transfer in G–C Watson–Crick DNA Base Pairs in Solution. *Angew. Chem. Int. Ed.* **2015**, *54*, 14719–14722.

(69) Röttger, K.; Marroux, H. J. B.; Chemin, A. F. M.; Elsdon, E.; Oliver, T. A. A.; Street, S. T. G.; Henderson, A. S.; Galan, M. C.; Orr-Ewing, A. J.; Roberts, G. M. Is UV-Induced Electron-Driven Proton Transfer Active in a Chemically Modified A·T DNA Base Pair? *J. Phys. Chem. B* **2017**, *121*, 4448–4455.

(70) Bull, G. D.; Thompson, K. C. Proton Transfer and Tautomerism in 2-Aminopurine–Thymine and Pyrrolocytosine–Guanine Base Pairs. *Biochemistry* **2018**, *57*, 4547–4561.

TOC Graphic

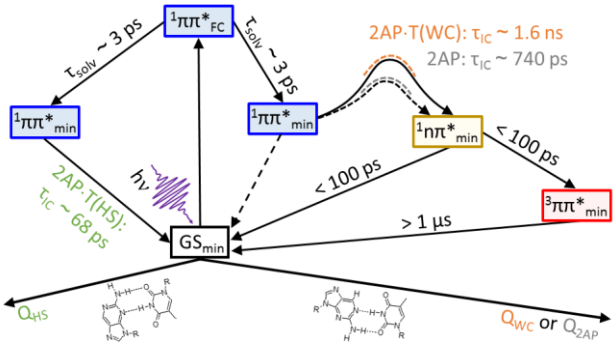
$^1\pi\pi^*_{FC}$
τ_{solv} ~ 3 ps
τ_{solv} ~ 3 ps
$^1\pi\pi^*_{min}$
$^1\pi\pi^*_{min}$
2AP·T(WC): τ_{IC} ~ 1.6 ns
2AP: τ_{IC} ~ 740 ps
$^1n\pi^*_{min}$
< 100 ps
$^3\pi\pi^*_{min}$
hν
2AP·T(HS):
τ_{IC} ~ 68 ps
< 100 ps
> 1 μs
GS_{min}
Q_{HS}
Q_{WC} or Q_{2AP}